Electronic Supplementary Material (ESI) for Journal of Materials Chemistry A.

SUPPORTING INFORMATION

Physicochemical and Electrochemical Characterization of Salt-in-Water and Water-in-Salt Potassium and Lithium Acetate Electrolytes

Mona Amiri and Daniel Bélanger*

Département de Chimie, Université du Québec à Montréal, Case Postale 8888, succursale Centre-Ville, Montréal, Québec, Canada H3C 3P8

* belanger.daniel@uqam.ca

Capacitance Studies

The capacitance (C) of the electrodes in different concentrations of potassium and lithium acetate electrolytes was calculated via averaging the capacitance at frequencies typically in the 10 to 1000 Hz range (where the phase angle approaches −90° indicating a capacitive behavior) using Eq. S1:[1]

$$C_A = \frac{1}{2\pi f Z'' A} \qquad \text{Eq. S1}$$

where f is the applied frequency, Z'' is the imaginary part of the impedance, and A is the surface area of the working electrode.

Diffusion Coefficient of the Redox Probe

The diffusion coefficient of the ferricyanide redox species was investigated through chronoamperometry in electrolytes containing 10 mM $K_3Fe(CN)_6$, where potential was stepped from initial value of 0.6 V (at which no reduction occurs) to 0 V and held for 10 s. The corresponding diffusion coefficient was calculated using the slope of fitting line in the chronoamperograms with current response plotted vs. $t^{-1/2}$ and the following Cottrell equation (Eq. S2):[2]

$$i = \frac{nFAc\sqrt{D}}{\sqrt{\pi t}} \qquad \text{Eq. S2}$$

where *n* is number of electrons transferred per molecule (*n* = 1), *A* is the surface area of the working electrode, *F* is the Faraday constant (96485 C mol^{-1}), and *c* is the initial bulk concentration of the $K_3Fe(CN)_6$ (10 mM). For comparison purposes, the diffusion coefficients were also calculated by plotting the peak currents (i_p) vs. the square root of scan rate obtained from the CVs and applying the Randles-Sevčik equation (Eq. S3):[2]

$$i_p = 0.4463nFAc\left(\frac{nF\upsilon D}{RT}\right)^{1/2} \qquad \text{Eq. S3}$$

where υ is the scan rate, *R* is the molar gas constant (8.314 J mol^{-1} K^{-1}) and *T* is absolute temperature (298 K here). Diffusion coefficient of ferrocene methanol (3.5 mM) was calculated using the CVs obtained at various scan rates.

Heterogeneous Electron Transfer Kinetics

The heterogeneous electron transfer kinetics of the ferricyanide/ferrocyanide and ferrocene methanol/ferrocenium methanol redox reactions is also investigated by finding the dimensionless kinetic parameter (ψ)[3] via ΔE_p of Figure 4A and 5B extracted from the corresponding cyclic voltammograms. The standard heterogeneous rate constant (k^0) was then determined via Nicholson and Shain Eq. S4 [2]:

$$\psi = k^0\left(\frac{D_O}{D_R}\right)^{\alpha/2}\sqrt{\frac{RT}{\pi nF\upsilon D_O}} \qquad \text{Eq. S4}$$

where α is the transfer coefficient (α = 0.5 here), D_O and D_R are the diffusion coefficient of the oxidized and reduced components (considered equal here), respectively.[4]

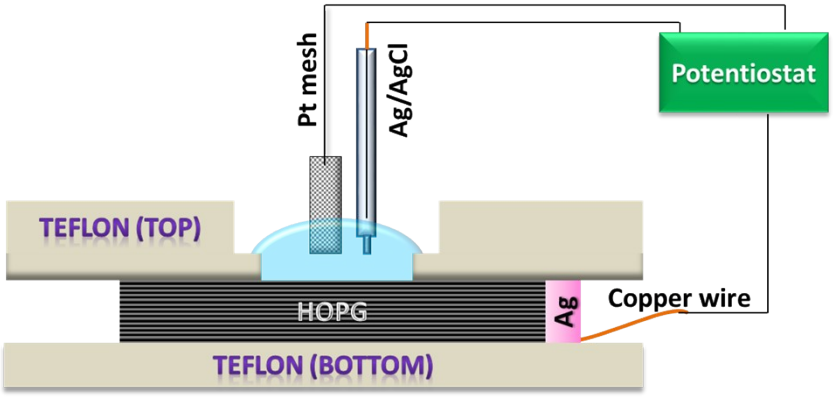

Scheme S1. Schematic illustration of the electrochemical three-electrode cell setup used for experiments carried out on highly oriented pyrolytic graphite (HOPG) electrode.

Table S1. Physicochemical properties of the potassium and lithium acetate electrolytes at room temperature.

Electrolyte	C (m)	C (M)	Salt molar fraction (%)	Density (g cm^{-3})
KOAc	1	0.98	1.77	1.08 ± 0.03
	10	6.35	15.27	1.27 ± 0.02
	27	10.29	32.73	1.40 ± 0.01
LiOAc	1	0.97	1.75	1.03 ± 0.01
	8	5.94	12.43	1.15 ± 0.01
KOAc + LiOAc	32 + 8	9.74 + 2.41	41.84	1.43 ± 0.01

The values reported for potassium acetate electrolytes are in good agreement with the literature.[5]

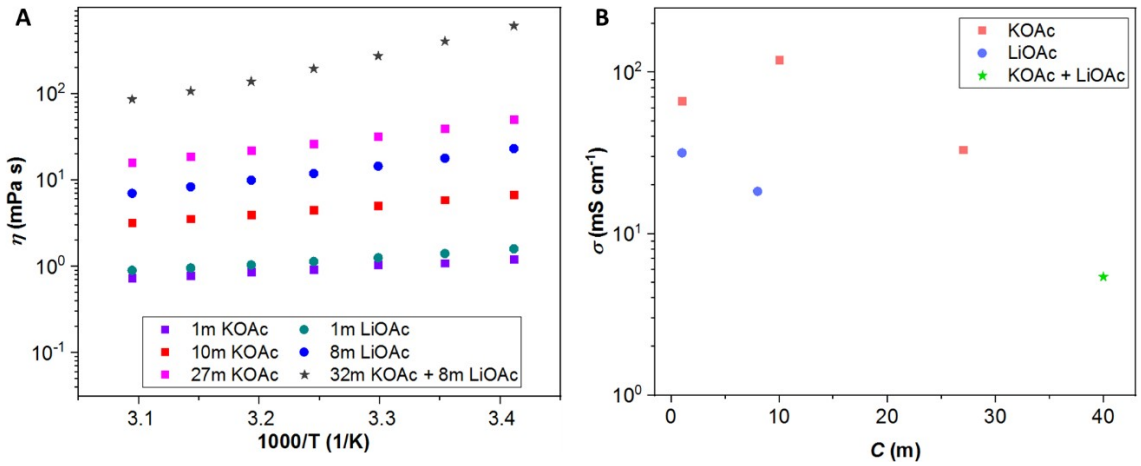

Figure S1. Viscosity values as a function of temperature varying between 21-50 °C (A) and ionic conductivity values at 25 °C (B) for the potassium and lithium acetate electrolytes.

The values reported for potassium acetate electrolytes are in good agreement with the literature.[5]

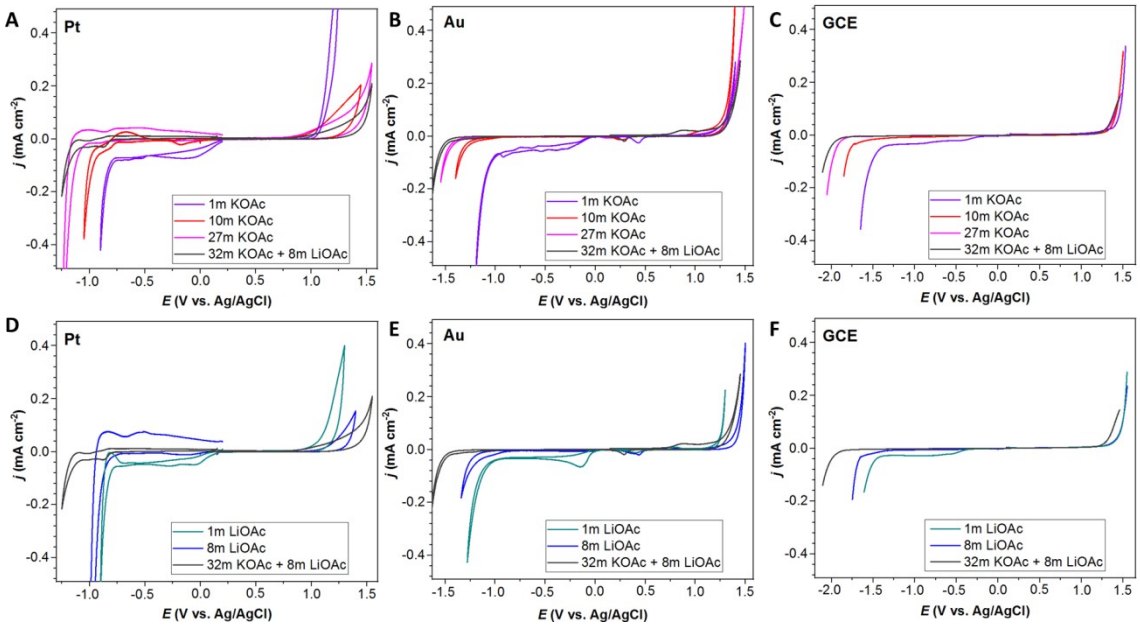

Figure S2. Experimental recorded cyclic voltammograms of Pt and Au electrodes, and linear sweep voltammograms of glassy carbon electrode in potassium (A-C) and lithium (D-F) acetate electrolytes as shown in Figure 1. (25 ^{o}C; scan rate of 1 mV s^{-1}).

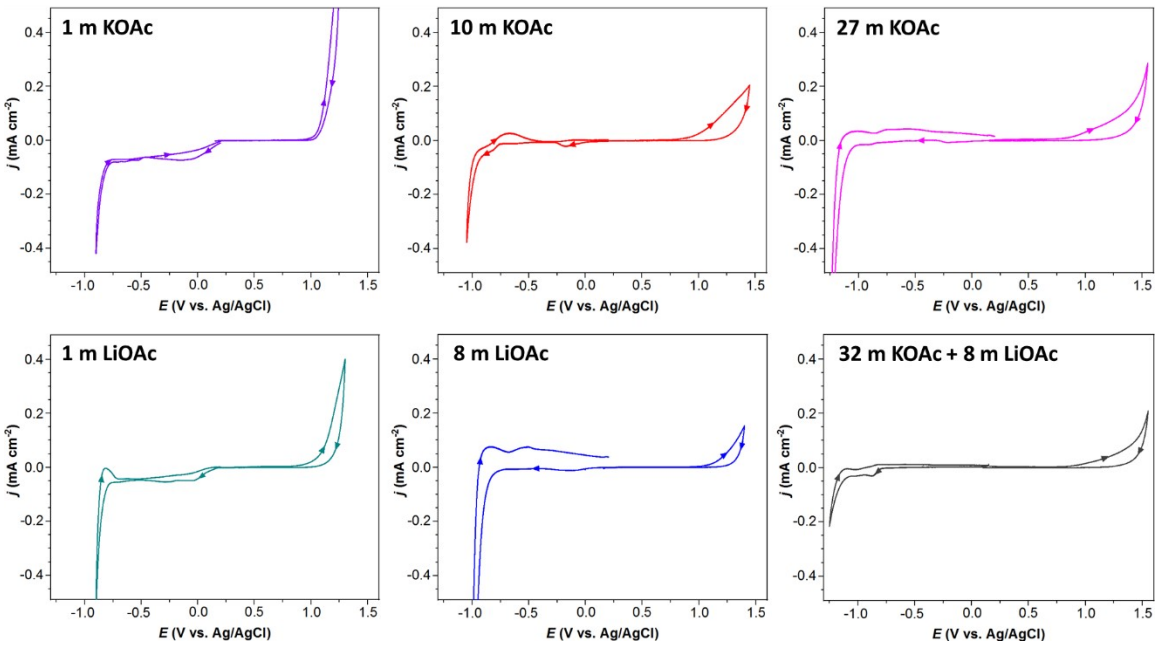

Figure S3. Cyclic voltammograms of Pt electrode in the potassium and lithium acetate electrolytes at 25 ^{o}C (starting at 0.15 V, cycling in the positive potential direction, sweep reversal to a negative potential limit and return to the initial potential; scan rate = 1 mV s^{-1}).

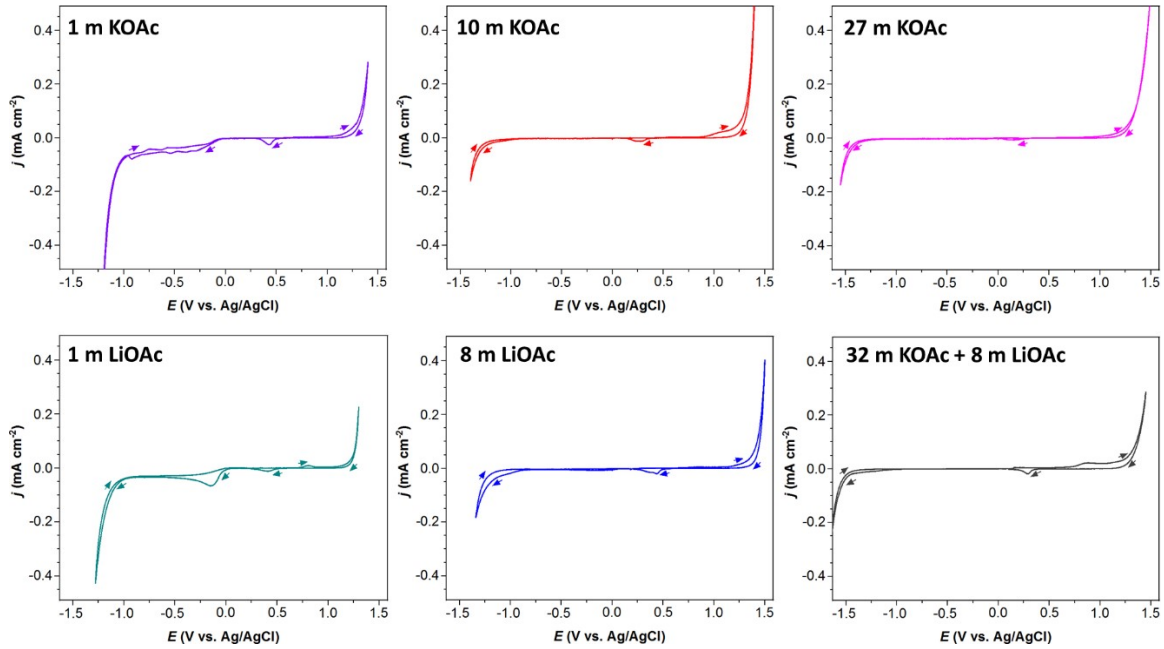

Figure S4. Cyclic voltammograms of Au electrode in the potassium and lithium acetate electrolytes at 25 ^{o}C (starting at 0.15 V, cycling in the positive potential direction, sweep reversal to a negative potential limit and return to the initial potential; scan rate = 1 mV s^{-1}).

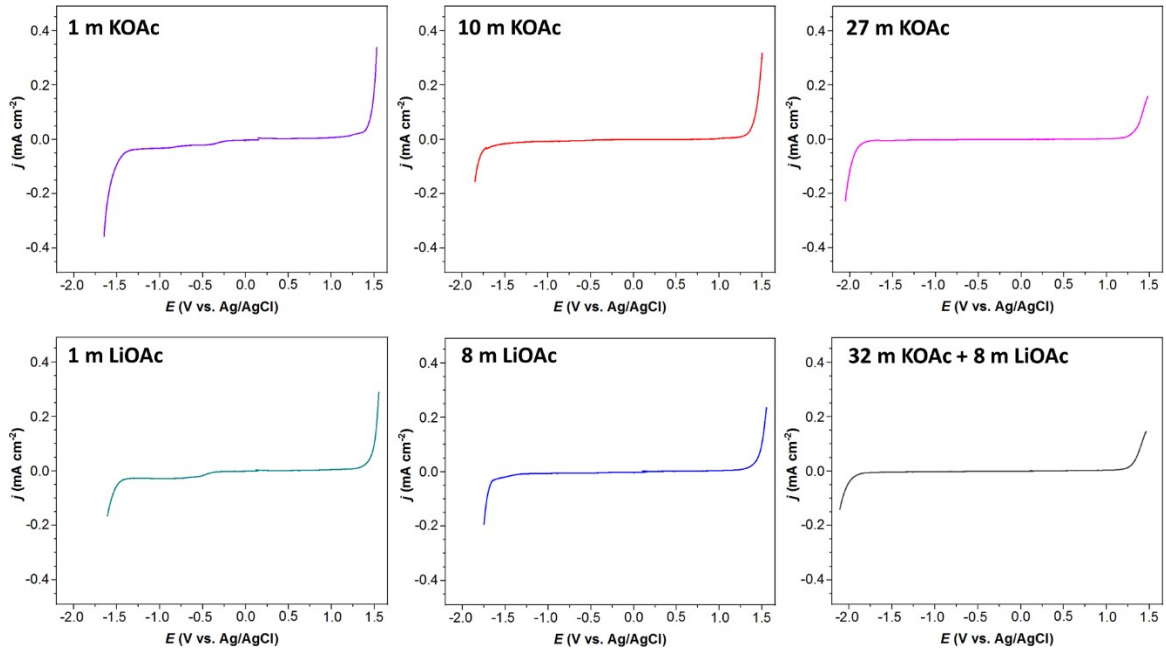

Figure S5. Linear sweep voltammograms of glassy carbon electrode in the potassium and lithium acetate electrolytes at 25 °C (starting at 0.15 V, sweeping in the positive potential direction first, then towards negative potential limit).

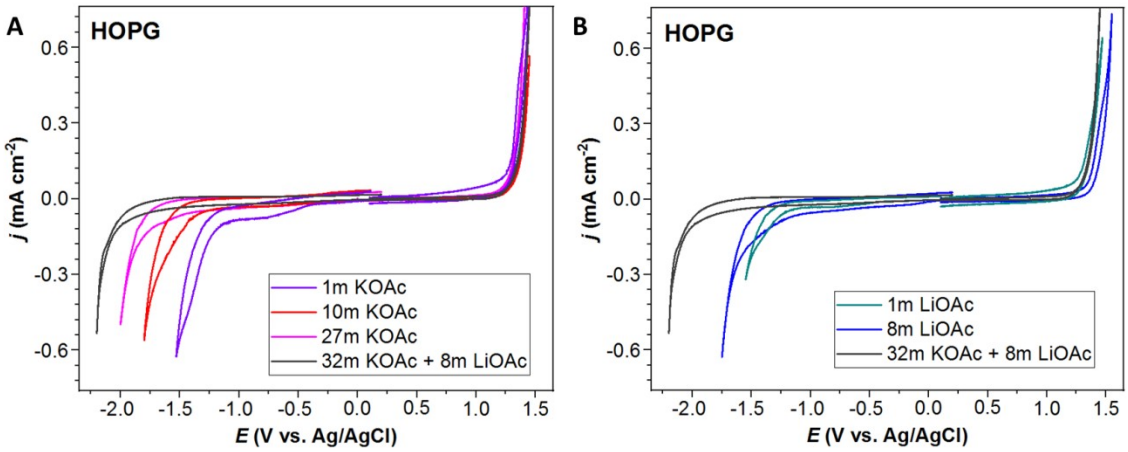

Figure S6. Experimental recorded cyclic voltammograms of highly oriented pyrolytic graphite (HOPG) electrode in potassium (A) and lithium (B) acetate electrolytes as shown in Figure 2. (Ar; 25 ^{o}C; scan rate of 200 mV s^{-1}).

Table S2. Experimental values of the onset potential for the hydrogen (HER) and oxygen (OER) evolution reactions at glassy carbon, Au, Pt, Au and HOPG electrodes in the various acetate electrolytes and their pH together with the thermodynamic values of the potential of the hydrogen and oxygen reactions at the pH of the electrolytes.

Electrolyte (pH)	**Onset Potential (V vs. Ag/AgCl) HER/OER**				**E (H^+-H_2)/E (O_2-H_2O) (V vs. Ag/AgCl)**
	Glassy Carbon	**Au**	**Pt**	**HOPG**	
1 m KOAc (8.5)	-1.39/1.36	-0.97/1.21	-0.75/1.04	-1.15/1.21	-0.71/0.52
10 m KOAc (10.5)	-1.70/1.33	-1.21/1.20	-0.90/1.25*	-1.39/1.24	-0.83/0.40
27 m KOAc (11.0)	-1.86/1.28	-1.39/1.21	-1.04/1.42	-1.60/1.21	-0.86/0.37
1 m LiOAc (8.0)	-1.42/1.37	-1.00/1.20	-0.77/1.14*	-1.22/1.22	-0.68/0.55
8 m LiOAc (8.5)	-1.65/1.37	-1.17/1.34	-0.79/1.28*	-1.35/1.35	-0.71/0.52
32 m KOAc + 8 m LiOAc (11.0)	-1.90/1.28	-1.45/1.25	-1.10/1.46	-1.85/1.22	-0.86/0.37

* The reverse scan was used.

**The thermodynamic potential values were estimated by the Nernst equation assuming that the activity of water is equal to 1.

Table S3. Electrochemical stability window (ESW) of the potassium and lithium acetate-based electrolytes at 2 different current cut-offs using voltammograms presented in Figures 1 and 2.

Electrolyte	ESW (V); 0.01 mA cm^{-2} cut-off			ESW (V); 0.1 mA cm^{-2} cut-off			ESW (V); 0.1 mA cm^{-2} cut-off
	GCE	Au	Pt	GCE	Au	Pt	HOPG
1 m KOAc	1.42	1.23	0.80	2.98	2.38	1.90	2.38
10 m KOAc	2.53	2.02	1.45	3.25	2.66	2.18	2.72
27 m KOAc	3.08	2.38	1.69	3.41	2.85	2.46	2.96
1 m LiOAc	1.73	1.17	0.81	3.06	2.40	1.96	2.61
8 m LiOAc	2.63	2.13	1.83	3.21	2.70	2.21	2.68
32 m KOAc + 8 m LiOAc	3.09	2.01	1.76	3.48	2.93	2.63	3.31

Table S4. Electrochemical stability window of the potassium and lithium acetate-based electrolytes found in the literature.

Electrolyte	C (m)	ESW (V)	Cut-off (mA cm^{-2})	Electrode	Ref
KOAc	1	1.4	0.01	Al/Ti	6
		1.55	0.1	Pt	7
		2.35	0.1	GC	5
	10	2.4	0.01	Al/Ti	6
		2.5	0.1	GC	5
	27	2.7	0.1	Pt	7
LiOAc	7	2.3	-	Ti foil	8
KOAc + LiOAc	32 + 8	2.7	0.1	Pt	7

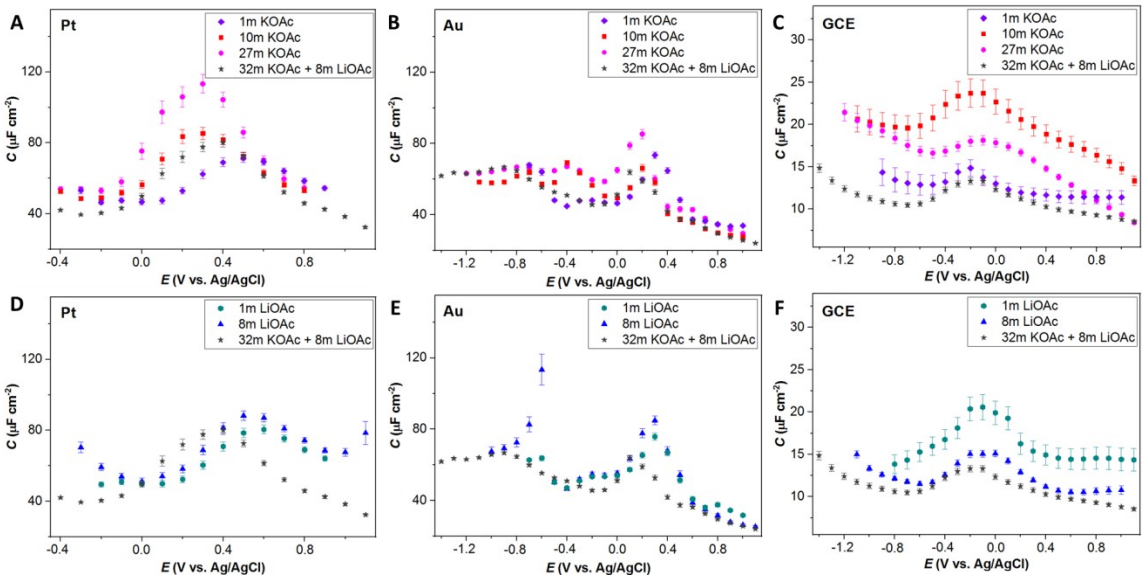

Figure S7. C-E curves of Pt, Au, and GCE working electrodes obtained from electrochemical impedance spectroscopy measurements in potassium (A-C) and lithium (D-F) acetate electrolytes of different concentrations at 25 °C, under Ar (measurements started at the most negative potential (depending on the electrolyte) and potentials were swept in anodic direction).

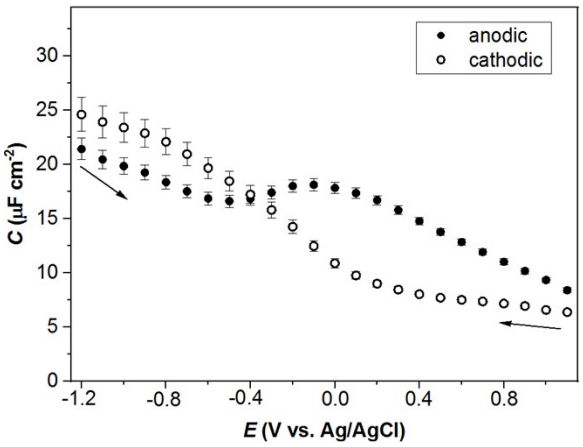

Figure S8. The effect of potential sweeping direction on hysteresis in C-E curves obtained by EIS measurements in a 27 m KOAc electrolyte at 25 ^{o}C, under Ar (GCE working electrode was polished in between the experiments).

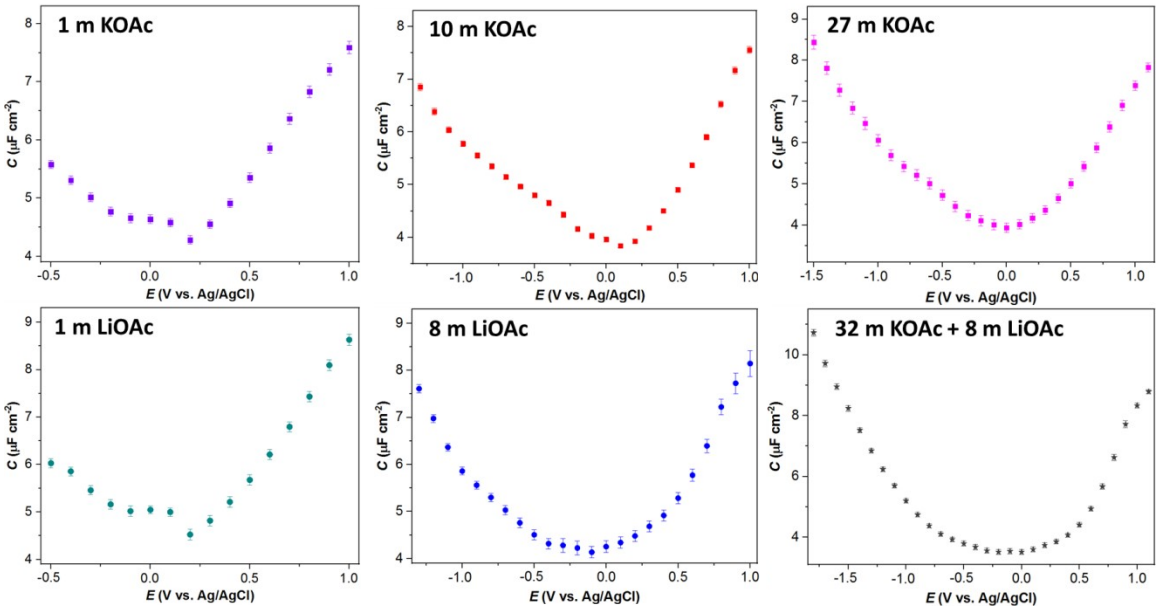

Figure S9. Capacitance-potential plots of HOPG working electrode in the potassium and lithium acetate electrolytes of various concentrations presented in Figure 3.

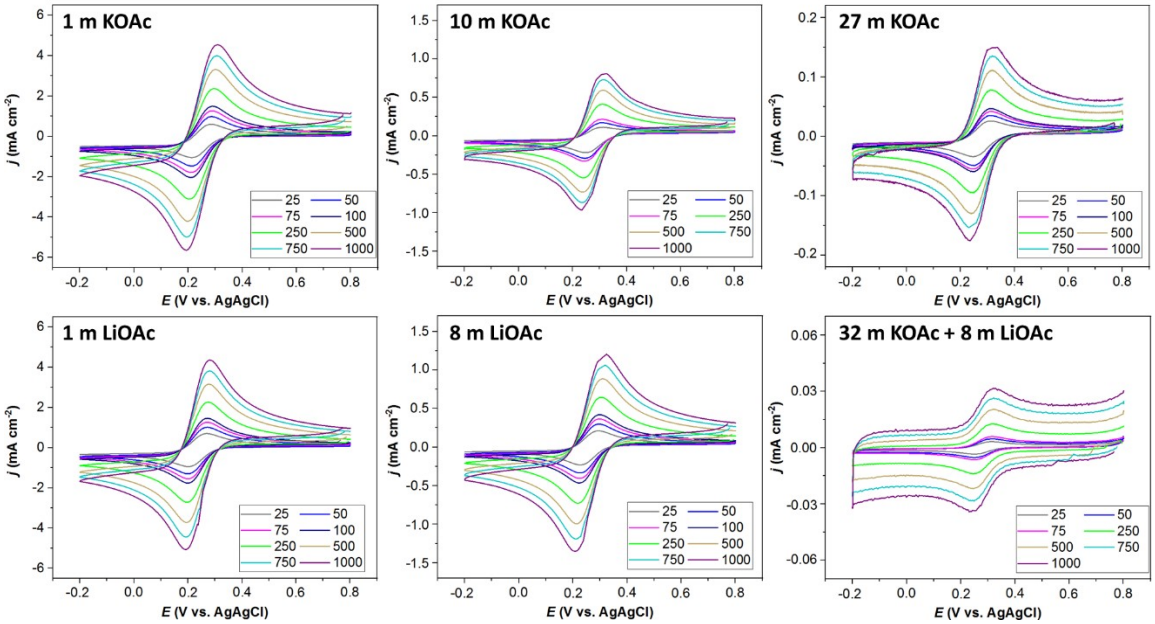

Figure S10. Cyclic voltammograms of glassy carbon electrode in acetate electrolytes containing 10 mM $K_3Fe(CN)_6$ under Ar at 25 ^oC; scan rate 25-1000 mV s^{-1}.

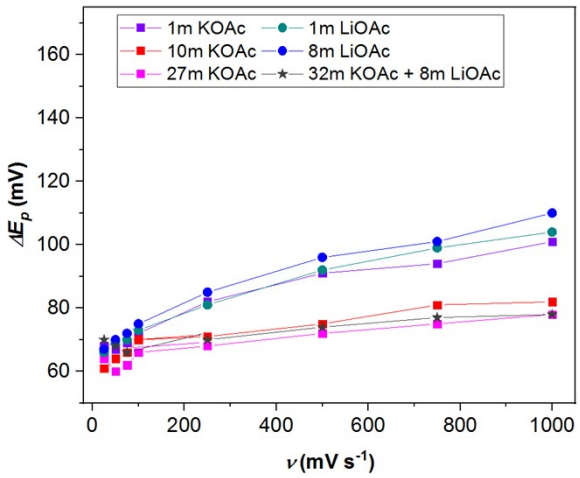

Figure S11. Peak separation of the voltammograms shown in Figure S10 as function of scan rate for the potassium and lithium acetate electrolytes.

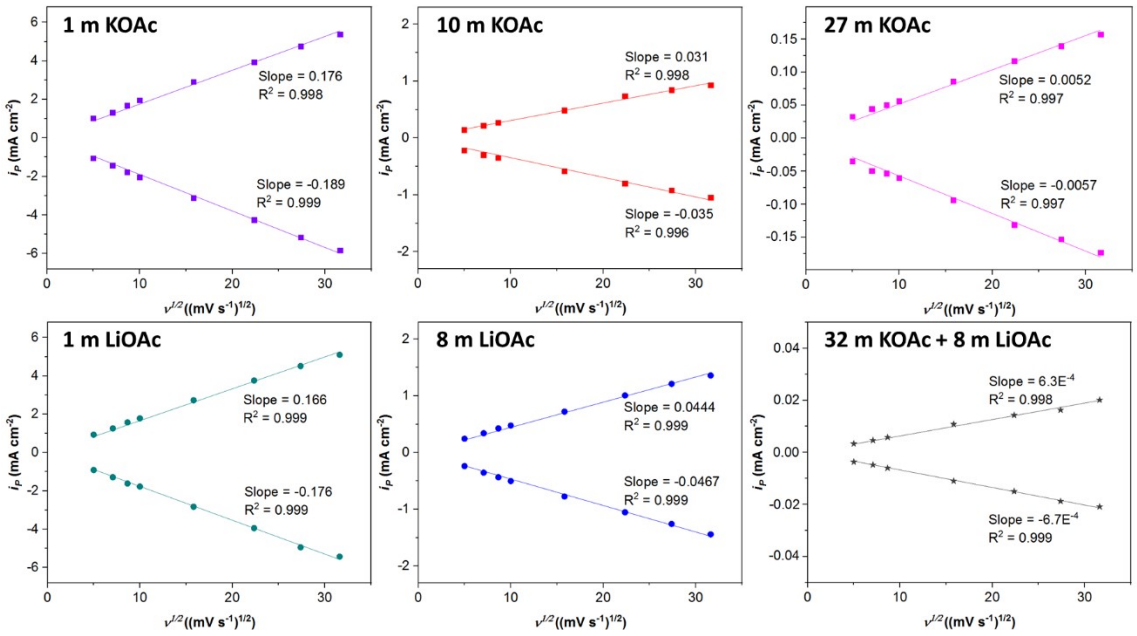

Figure S12. Correlation of peak current and square-root of scan rate for the potassium and lithium acetate electrolytes containing 10 mM $K_3Fe(CN)_6$ at 25 ^oC, under Ar (extracted from voltammograms shown in Figure S10; scan rate varying in the 25-1000 mV s^{-1} range).

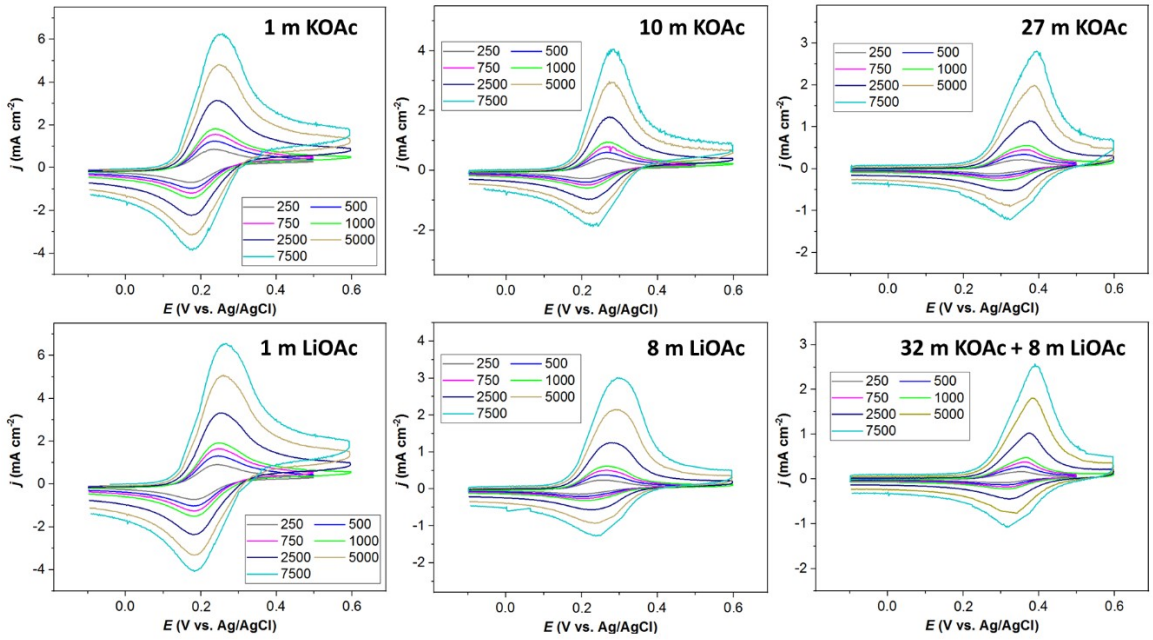

Figure S13. Cyclic voltammograms of glassy carbon electrode in acetate electrolytes containing 3.5 mM ferrocene methanol at 25 °C; scan rate 250-7500 mV s^{-1}.

Table S5. Apparent redox potential of ferrocene on glassy carbon for the LiTFSI electrolytes of various concentrations containing 2mM ferrocene.

C **(M)**	$E_{1/2}$ **(V vs. Ag wire)**
1	-0.16
2.5	-0.08
5	-0.03

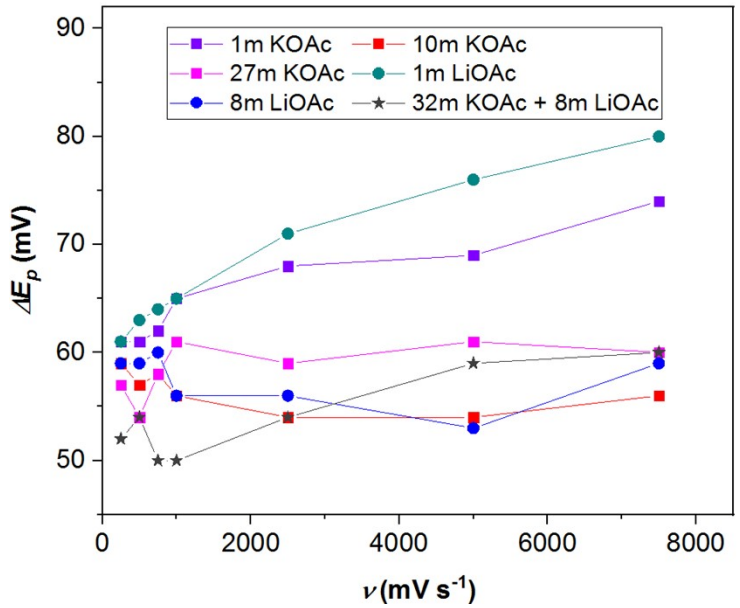

Figure S14. Peak separation of the voltammograms shown in Figure S13 as function of scan rate for the potassium and lithium acetate electrolytes containing 3.5 mM ferrocene methanol.

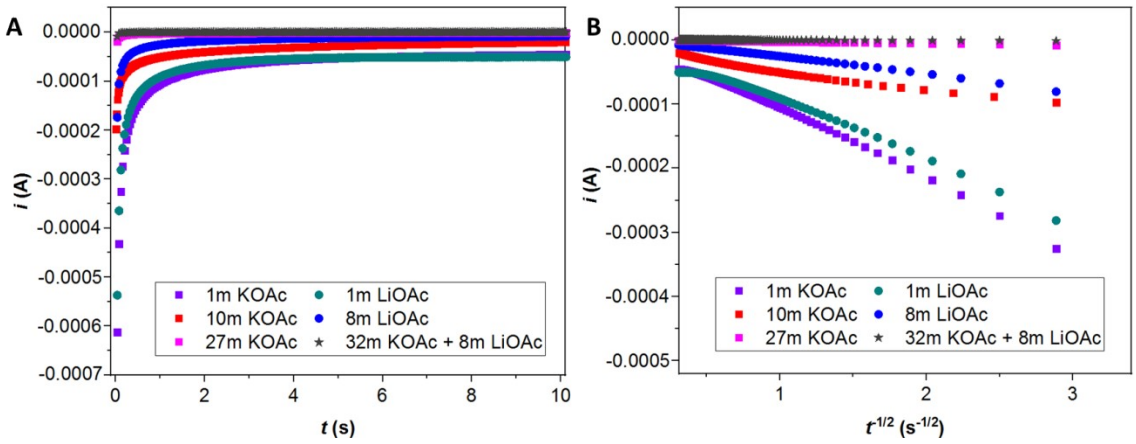

Figure S15. Diffusion coefficient study of $Fe(CN)_6^{3-}$ species using chronoamperometry; Current vs. time (A) and reverse square-root of time (B) after stepping potential from 0.6 to 0 V in the acetate electrolytes containing 10 mM $K_3Fe(CN)_6$ under Ar at 25 ^oC (glassy carbon electrode).

The GC electrode was held at 0.6 V for 10 s then the potential was stepped to 0 V (held for 10 s), where it is expected that ferricyanide gets reduced to form ferrocyanide and the process is controlled by diffusion. All the electrolytes demonstrate a good linearity between current and inverse square root of time. The slope of the fitted line decreases with increase in concentration for potassium and lithium electrolytes, indicating a lower ion diffusion caused by higher viscosity. Applying the data found from these curves to Cottrell equation, diffusion coefficient (D) of $K_3Fe(CN)_6$ in the acetate electrolytes can be determined.[2]

Table S6. Summary of the diffusion coefficients of ferricyanide (D) and standard electron transfer rate constants (k^0) using Cottrell and Randles-Sevčik equations for the ferricyanide/ferrocyanide redox system in the acetate electrolytes of various concentrations.

Electrolyte	***C* (m)**	**Cottrell**		**Randles-Sevčik**	
		D **(10^{-6} cm^2 s^{-1})**	***k*^{0}** **(10^{-3} cm s^{-1})**	***D*** **(10^{-6} cm^2 s^{-1})**	***k*^{0}** **(10^{-3} cm s^{-1})**
KOAc	1	6.03 ± 0.32	16.88 ± 0.98	4.96	15.31 ± 0.89
	10	0.78 ± 0.04	13.43 ± 2.55	0.16	6.08 ± 1.16
	27	0.005 ± 0.001	1.87 ± 0.60	0.004	1.68 ± 0.54
LiOAc	1	4.50 ± 0.71	13.93 ± 0.49	4.30	13.62 ± 0.48
	8	0.41 ± 0.04	3.65 ± 0.11	0.30	3.12 ± 0.09
KOAc + LiOAc	32 + 8	$1.53E^{-4}$ ± $0.43E^{-4}$	0.15 ± 0.02	$0.6E^{-4}$	0.09 ± 0.01

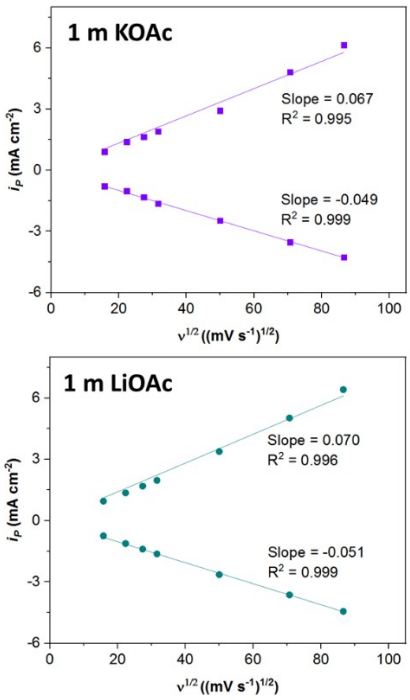

Figure S16. Correlation of peak current and square-root of scan rate for the potassium and lithium acetate electrolytes containing 3.5 mM ferrocene methanol at 25 ^{o}C (extracted from voltammograms shown in Figure S11; scan rate varying in 250-7500 mV s^{-1} range).

References

1. P. Iamprasertkun and R. A. Dryfe, in *Nanocarbon Electrochemistry,* "The Capacitance of Graphene: From Model Systems to Large-Scale Devices",ed. N. Yang, G. Zhao, J. Foord, John Wiley & Sons Ltd, Hoboken, New Jersey, 1st edition, 2020, chapter 2, 33-84.
2. A. J. Bard and L. R. Faulkner, *Electrochemical methods fundamentals and applications*, John Wiley & Sons Ltd, Hoboken, New Jersey, 2001.
3. R. S. Nicholson, "Theory and application of cyclic voltammetry for measurement of electrode reaction kinetics", *Anal. chem*., 1965, **37**, 1351-1355.
4. M. Velicky, D. F. Bradley, A. J. Cooper, E. W. Hill, I. A. Kinloch, A. Mishchenko, K. S. Novoselov, H. V. Patten, P.S. Toth, A. T. Valota and S. D. Worrall, "Electron transfer kinetics on mono-and multilayer graphene", *ACS Nano*, 2014, **8**, 10089-10100.
5. P. L. Stigliano, N. Pianta, S. Bonizzoni, M. Mauri, R. Simonutti, R. Lorenzi, B. Vigani, , V. Berbenni, S. Rossi, P. Mustarelli and R. Ruffo, "A physico-chemical investigation of highly concentrated potassium acetate solutions towards applications in electrochemistry", *Phys. Chem. Chem. Phys.*, 2021, **23**, 1139-1145.
6. D. P. Leonard, Z. Wei, G. Chen, F. Du and X. Ji, "Water-in-salt electrolyte for potassium-ion batteries", *ACS Energy Lett.*, 2018, **3**, 373-374.
7. M. R. Lukatskaya, J. I. Feldblyum, D. G. Mackanic, F. Lissel, D. L. Michels, Y. Cui and Z. Bao, "Concentrated mixed cation acetate “water-in-salt” solutions as green and low-cost high voltage electrolytes for aqueous batteries", *Energy Environ. Sci.*, 2018, **11**, 2876-2883.
8. S. Chen, R. Lan, J. Humphreys and S. Tao, "Effect of cation size on alkali acetate-based ‘water-in-bisalt’electrolyte and its application in aqueous rechargeable lithium battery", *Appl. Mater. Today*, 2020, **20**, 100728.